INVITED PAPER *Special Section on Recent Advances in Photonics Technologies and Their Applications*

Photonics for Millimeter-Wave and Terahertz Sensing and Measurement

Tadao NAGATSUMA[†a)], ***Fellow***, **Shintaro HISATAKE**[†], ***Member***,
and **Hai Huy NGUYEN PHAM**[†], ***Student Member***

SUMMARY This paper describes recent progress of photonically-enabled systems for millimeter-wave and terahertz measurement applications. After briefly explaining signal generation schemes as a foundation of photonics-based approach, system configurations for specific applications are discussed. Then, practical demonstrations are presented, which include frequency-domain spectroscopy, phase-sensitive measurement, electric-field measurement, and 2D/3D imaging.

key words: *millimeter wave, terahertz, photonics, spectroscopy, imaging, measurement*

1. Introduction

Measurement of high-frequency electrical signals using photonic techniques can be traceable back to late 1970s and early 1980s, when numerous methods to generate and detect picosecond electrical signals were developed using femtosecond pulse lasers such as mode-locked dye lasers and Nd:YAG lasers [1]–[3]. With advent of fiber-optic communications technologies, these pulse lasers were replaced with semiconductor lasers and fiber lasers in 1990s, which accelerated the development and commercialization of measurement and testing instruments for high-speed integrated circuits (ICs) [4], [5]. Also in early 1990s, terahertz (THz) spectroscopy [6] and imaging [7] techniques using THz pulses were developed, which made a great impact on the THz research as a trigger of its boom [8], [9]. THz time-domain spectroscopy and imaging systems using pulse lasers have been commercialized since 2000s. Now, one of the recent trends is a movement toward frequency-domain systems with continuous THz waves which enable higher sensitivity and more functionalities.

In this paper, we describe recent progress of measurement and sensing applications in the millimeter-wave and THz frequency regions based on frequency-domain photonic techniques using continuous waves. Section 2 overviews several schemes for photonic generation of continuous waves, and system configurations suitable to specific applications. Then, some of our recent applications are presented in Sect. 3 showing how effectively photonic techniques are employed in measurement and sensing systems.

Manuscript received July 17, 2015.
Manuscript revised October 4, 2015.
[†]The authors are with Osaka University, Toyonaka-shi, 560–8531 Japan.
a) E-mail: nagatuma@ee.es.osaka-u.ac.jp
DOI: 10.1587/transele.E99.C.173

2. Signal Generation and System Configurations

2.1 Signal Generation

Figure 1 show schematic diagrams for generating RF signals by means of photonic techniques. Figure 1 (a) depicts a free-running signal generator. First, intensity-modulated optical signals, whose envelope is sinusoidal at a designated RF frequency, are generated with use of two free-running lasers; a wavelength tunable laser and a wavelength-fixed laser operating at different wavelengths, λ_1 and λ_2. Then, these two-wavelength of lights are injected to optical-to-electrical (O/E) converters, which leads to the generation of THz waves at a frequency given by $f_{RF} = c|\lambda_1 - \lambda_2|/(\lambda_1 \cdot \lambda_2)$, where c is a velocity of light. This conversion process is often referred to as "photo-mixing." The converted signals are

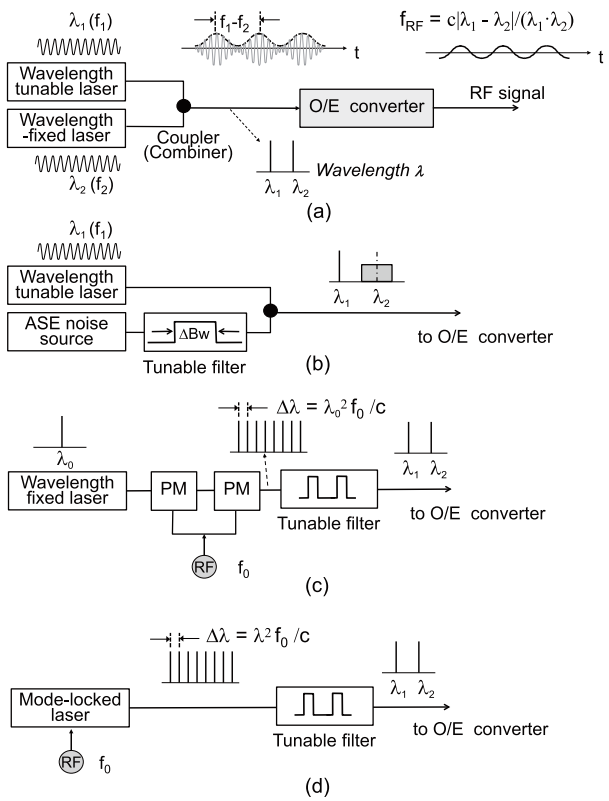

Fig. 1 Schematic diagrams of optically generated RF signal sources. PM: optical phase modulator.

finally radiated into free space by an antenna.

As for O/E converters, we use a uni-traveling-carrier-photodiode (UTC-PD), which satisfies both wide bandwidth and high output power [10]. The J-band UTC-PD module has a 3-dB bandwidth of over 100 GHz, and a typical output power of over 100 μW at 300 GHz for a photocurrent of 10 mA [11]. A photoconductive antenna is another well-known O-E converter, which can operate at THz frequencies, but is more suitable for the pulse generation with high peak current [12].

For many RF applications, noise sources are also important, but there has been a lack of high-power noise sources in the THz region. Figure 1 (b) shows a diagram of photonically generated noise sources with controlled bandwidth. Amplified spontaneous emission (ASE) noise from, for instance, a fiber laser and a superluminescent diode is first fed into an optical filter at a designated optical center wavelength λ_2 and a bandwidth ΔB_W. After being combined with a single frequency laser λ_1 in the PD, the noise signal with a bandwidth B at a frequency f_{RF} is generated.

When frequency and phase-stabilized RF signals are required, the use of optical frequency combs and actively mode locked lasers together with optical filters is an efficient way as shown in Figs. 1 (c) and 1 (d). The optical filters select two wavelengths among multiple wavelengths of lights whose frequency interval is determined by the frequency of an electrical signal source.

2.2 System Configurations

Table 1 summarizes several applications with different combination of signal sources and detectors, and their simplified configurations are illustrated in Fig. 2.

As for spectroscopy applications, frequency-domain systems using a photoconductor (PC) or a PD for both the signal generation and detection (Fig. 2 (a)) have been proven to offer higher dynamic range especially in the sub-THz region [13]. In addition, spectroscopic two-dimensional (2D) imaging of the object is feasible by scanning a THz beam over the object [14]. One of the great advantages of this approach is a capability of simultaneous measurement of amplitude and phase of THz waves passing through the object [15], [16].

Similar configuration is applicable to the electric-field measurement as shown in Fig. 2 (b) [17], [18]. In this case, the electro-optic (EO) crystal is used as an electric-field sensor in the detection. By using a large-area sensor, the EO measurement technique can be extended to a "camera"-like system, which enables 2D movie for the diagnosis of dynamic behavior of electro-magnetic waves [19]. Antenna characterization is one of the killer applications of this approach because of its extremely low invasiveness [20]–[22].

Figure 2 (c) shows another type of imaging system using a PD as the generator and a Schottky-barrier diode (SBD) as the detector. Even when the SBD is used as a simple direct detection receiver, it offers a relatively high sensitivity in the measurement. When we configure the interferometric or homodyne system, the system can be extended to three-dimensional (3D) tomographic imaging system [23]–[25].

In the next section, we will describe more detailed systems based on the above approaches.

Table 1 Combination of signal generators and detectors for different applications.

Application	Generation	Detection	Merits
Spectroscopy	Photoconductor Photodiode	Photoconductor Photodiode	Simultaneous measurement of amplitude and phase
Electric-field measurement	Photodiode	Electro-optic crystal	Low invasiveness
2D/3D imaging	Photodiode	Schottky-barrier diode	Broadband simple

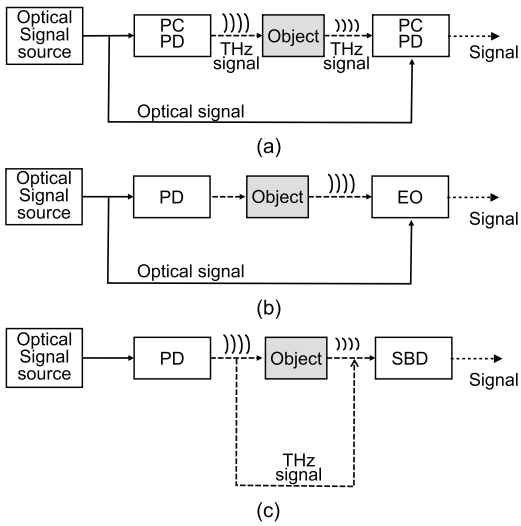

Fig. 2 Simplified configuration of measurement systems. (a) spectroscopy. (b) electric-field measurement. (c) imaging/tomography. In (c), an interferometric system is used for 3D imaging. PD: photodiode, PC: photoconductor, EO: electro-optic crystal, SBD: Schottky barrier diode.

3. Application Demonstrations

3.1 Spectroscopy

Figure 3 shows the THz frequency-domain spectrometer (THz-FDS) based on the configuration of Fig. 2 (a) using a self-heterodyne technique [15]. Two laser diodes (LDs) were used both for the generation and detection of the THz wave. A continuous THz wave was generated by O/E conversion at the UTC-PD. The THz wave passed through a sample was detected via mixing with an optical beat signal (optical local oscillator signal: LO). The frequency of the tunable LD was shifted with an optical frequency shifter (FS) to realize the self-heterodyne detection. The frequency-converted intermediate frequency (IF) signal was amplified with the transimpedance amplifier (TIA) and detected by the lock-in amplifier (LIA). In the self-heterodyne system, the frequency fluctuation of the RF signal, generated

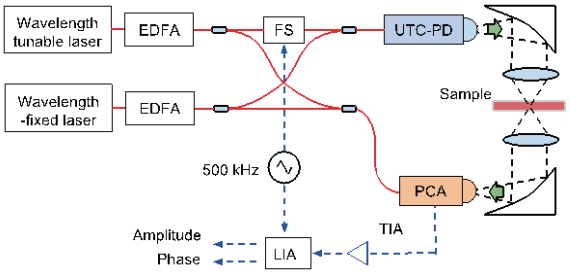

Fig. 3 THz-FDS based on the self-heterodyne technique. The THz wave is generated via E/O conversion at the uni-travelling-carrier photodiode (UTC-PD) and detected by the photoconductive antenna (PCA). EDFA: erbium-doped fiber amplifier, FS: frequency shifter, TIA: transimpedance amplifier, and LIA: lock-in amplifier.

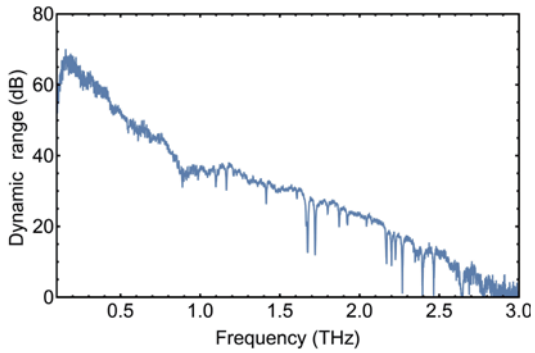

Fig. 4 Typical system response of the THz-FDS based on the self-heterodyne technique. Absorption spectra due to water vapor at over 1 THz were clearly observed.

by the UTC-PD and that of the optical LO signal has the same property, thus the frequency fluctuations of the free-running lasers are cancelled out via the mixing operation. In this system, the amplitude and phase of the THz wave can be measured simultaneously. The RF frequency can be tuned by changing the difference frequency between two lasers.

Figure 4 shows the typical system response. The UTC-PD was biased at −1.0 V. The optical power injected to the UTC-PD and the PCA was 13 dBm. The lock-in time constant was 10 msec. The maximum dynamic range of the system was about 70 dB at 200 GHz. The bandwidth of the system exceeds 2.5 THz. Absorption spectra by water vapor were observed.

3.2 Phase Sensing

Although the laser phase fluctuations are canceled out in the detection process, the conventional self-heterodyne system shows phase instabilities or phase drift due to the optical phase fluctuations imposed in the optical fibers. This problem can be solved by the balanced self-heterodyne system shown in Fig. 5 [23]. In the balanced self-heterodyne system, THz wave is divided into two paths. Each amplitude and phase detected by two mixers is measured by a two-channel dual-phase lock-in amplifier. After the detection, the common phase noises are subtracted ($\theta = \theta_2 - \theta_1$).

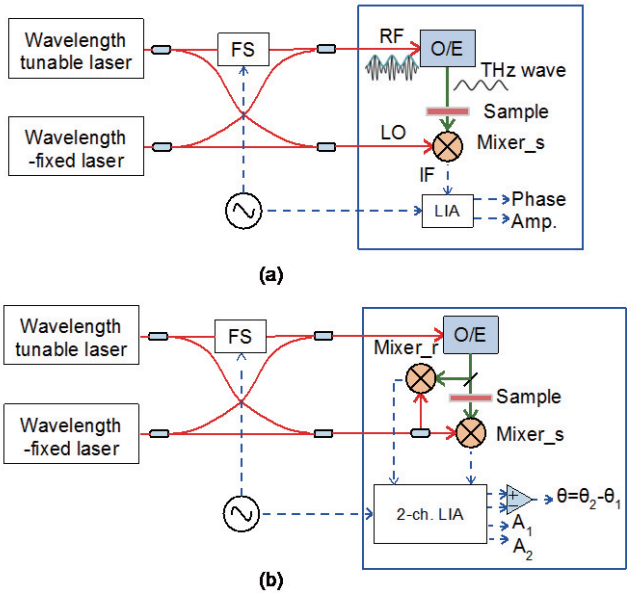

Fig. 5 Schematic diagrams of the conventional self-heterodyne system (a) and the balanced self-heterodyne system (b). LIA: lock-in amplifier.

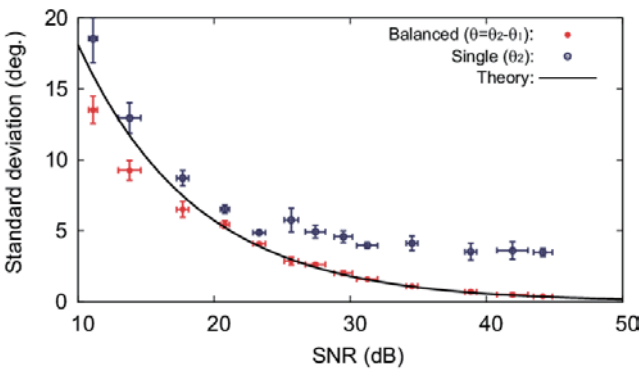

Fig. 6 Relation between the standard deviation of the detected phase and the SNR of the detected amplitude.

Figure 6 shows the relation between the signal-to-noise ratio (SNR) of the amplitude measurement and phase standard deviation [23]. The closed red circles are the results obtained with the balanced self-heterodyne system whereas the open circles are the data obtained without subtracting (conventional self-heterodyne system). The solid line is the theoretical relation. The phase standard deviation in the balanced self-heterodyne system was well fitted to the theoretical curve. This result indicates that the development of high-power THz generators and/or highly sensitive THz mixers will improve the sensitivity in not only the absorbance measurement but also the phase measurement.

At the point frequency of 380 GHz, the balanced self-heterodyne system was tested to demonstrate the phase contrast imaging as shown in Fig. 7 [24]. The minimum detectable optical path length change is proportional to the standard deviation of the phase measurement and inversely proportional to the THz frequency. However, the phase stan-

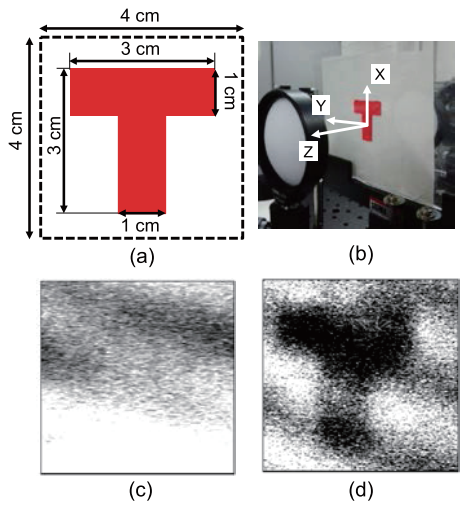

Fig. 7 (a) Dimensions of the letter "T", (b) sample mounted on the stage, (c) absorption-contrast image, and (d) phase-contrast image.

dard deviation decreases when the THz frequency increases. The phase imaging application was demonstrated at a frequency of 380 GHz because the minimum detectable optical path length of our system at this frequency is the smallest. The sample was a letter "T" written in red ink on 90-μm-thick paper. The THz wave was focused using Teflon lens. The sample was moved in the XY plane at the focal plane as shown in Fig. 7 (b). The spatial resolution was estimated to be 3.8 mm. Figures 7 (c) and (d) show the results of the absorption-contrast imaging and the phase-contrast imaging, respectively. The absorbance of the red ink was too small to resolve the letter "T", whereas the phase-contrast imaging clearly shows the letter "T". The balanced self-heterodyne system is suitable for the precise phase measurement.

3.3 Electric-Field Visualization

Visualization of the field evolution of the continuous waves with high phase and spatial resolution is a new approach to the study of the physical dynamics of unique beams, such as non-diffractive, self-reconstructing, and vortex beams. As near-field visualization can reveal device dynamics, it is also useful for diagnosing the THz devices. We have recently developed electric-field visualization system based on the configuration of Fig. 8 (a) using a nonpolarimetric self-heterodyne EO detection technique [18]. The field visualization system is similar to the self-heterodyne spectrometer shown in Fig. 3, except for the field detection using EO sensor. The incoming probe beam was fed to the EO sensor. After interacting with the THz waves in the EO crystal, the reflected outcoming beam passed through an optical filter and detected by a photodiode (PD). In this experiment, the frequency of the THz wave emitted from the horn antenna was set at 125 GHz because the THz power emitted from our generator was maximum at this frequency. The principle of the EO detection is based on the coherent detection of the modulation sideband generated in the EO crystal (ZnTe) via the interaction between the THz wave and the optical probe beam (Fig. 8 (b)). Unlike conventional EO detection schemes based on the polarization modulation where the sensitivity of the measurement can fluctuate drastically due to the fluctuation of the polarization state of the probe beam in the fiber, the nonpolarimetric EO detection scheme offers stable measurements.

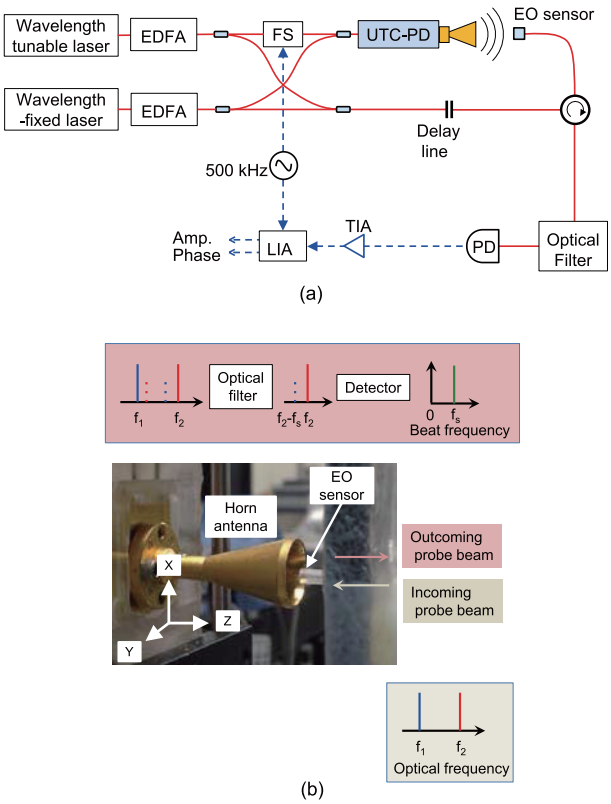

Fig. 8 Schematic of electric-field visualization system (a) and measurement principle the system (b). The THz wave is generated via a UTC-PD and detected by an electro-optic (EO) sensor. EDFA: erbium-doped fiber amplifier, FS: frequency shifter, PD: photodiode, TIA: transimpedance amplifier, and LIA: lock-in amplifier.

Figure 9 shows the visualized 3D distributions of the freely propagating wave. The amplitude data were normalized to their maximum values in each plane. The scan area (20λ = 50 mm) has been limited by the mechanical stage. The measured field distributions agreed well with those of simulations even for the near-field measurement, which verifies that our EO sensor is non-invasive in the measurement. It must be mentioned that the self-heterodyne technique is very effective to achieve a long phase stability during the measurement even with the use of free-running LDs.

3.4 Antenna Characterization

An antenna characterization method based on the near-field measurement, which was initially proposed in the microwave region [25], is an important and useful method also in millimeter-wave and THz regions because of a better SNR

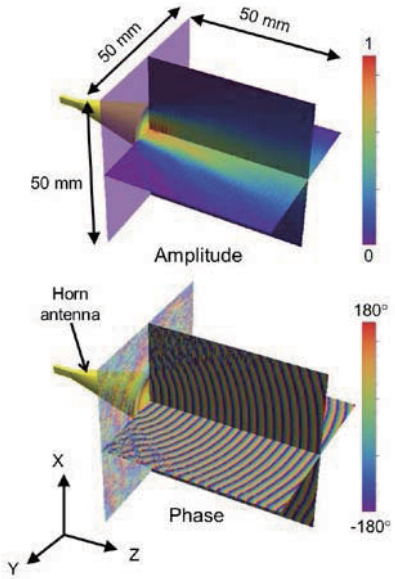

Fig. 9 Three-dimensional distributions of the freely propagating wave measured at 125 GHz.

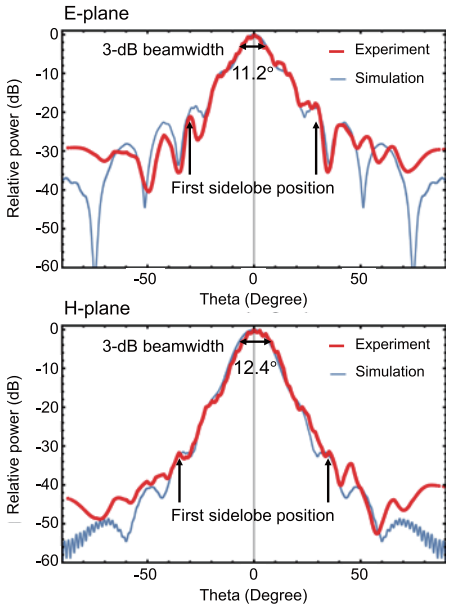

Fig. 10 Radiation pattern of the horn antenna at 125 GHz in E- and H-planes.

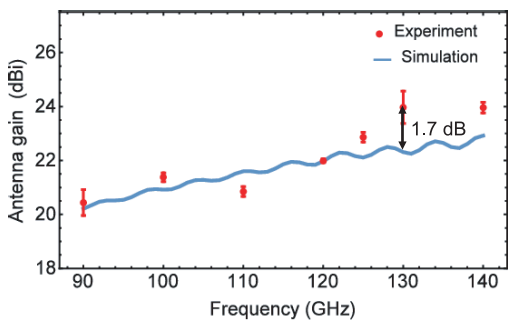

Fig. 11 Frequency characteristics of the antenna gain calculated from experimentally obtained 3-dB beam width.

in comparison with the far-field measurement. The Fourier transform of the near-field measurement was used in this method to determine the far-field radiation patterns. The characterization of F-band (90–140 GHz) standard horn antenna based on near-field measurement by our EO detection system is presented [22].

The amplitude and phase, measured in XY-plane (Fig. 9) was used for the determnation of radiation patterns. The measured plane was at the distance 0.5 mm from the horn antenna surface, which belongs to the radiating near-field region. This region is satisfied the condition for determining radiation patterns from the near-field measurement [25]. The THz power emitted from the horn antenna was 1.3 mW at the frequency of 125 GHz. The maximum SNR of the amplitude measurement was 40 dB and obtained at the center of the surface of the horn antenna with the lock-in time constant of 30 msec.

Figure 10 shows the experimental results in thick red lines and simulated results in thin blue lines of the radiation patterns of the horn antenna at 125 GHz. The main lobes and first sidelobes in the experiment agree well with those in the simulation for both E- and H-planes. The average of 5 experimental measurements of 3-dB beam widths are 11.2° and 12.4° in the E- and H-planes, respectively; whereas those in the simulated results are 11.5° and 13.6°, respectively. The sidelobes at the angle beyond the first sidelobes in the experiment are slightly different from those in the simulation. One of possible reasons of the disagreements is the limitation of the SNR of the near-field measurement. The gain of the horn antenna, calculated from the 3-dB beam widths, at 125 GHz is 22.8 dBi in the experiment and the results of simulation is 22.1 dBi. Figure 11 shows the frequency characteristics of the antenna gain. The red dots are the experimental results, while the blue solid curve is the simulated result. The experimental results agree well with the simulated result within 1.7 dB in the full F-band. This indicates our EO detection system can be applied to characterize indoor communication antennas, which has gain of about 23 dBi.

3.5 2D Imaging

Millimeter-wave and THz imaging has been extensively studied and deployed in numerous areas such as material inspection, non-destructive testing, and security applications [26]–[29]. Between CW and pulsed-wave imaging systems, the CW imaging can be faster, more compact, cost-effective and simpler to operate.

One of the drawbacks in the 2D-CW imaging using mono-chromatic coherent sources is degradation in image quality due to interference patterns caused by reflection of waves at any boundary in the object under inspection and components used such as lenses and mirrors, which leads to decrease in effective lateral spatial resolution.

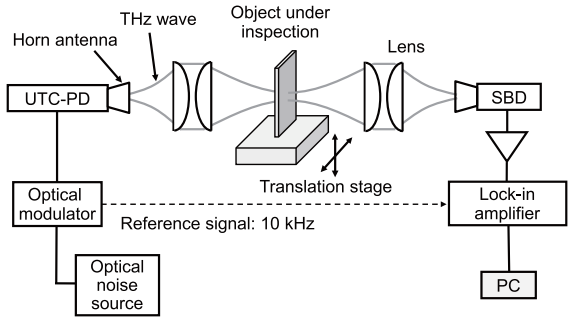

Fig. 12 Block diagram of a THz imaging system using low-coherence noise source.

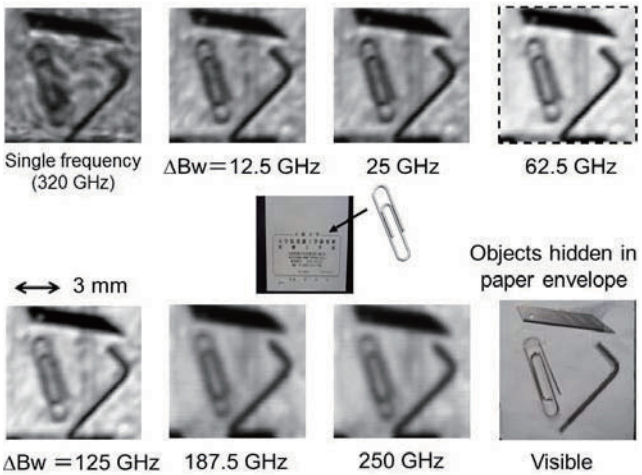

Fig. 13 2D images measured by changing the noise bandwidth, ΔB_W.

Figure 12 shows a block diagram of transmission-type THz imaging system based on the configuration of Fig. 2 (c) using a low-coherence THz noise source of Fig. 1 (b) [30]. The noise is radiated into free space via a horn antenna from the UTC-PD module, and it is focused onto the object under test with dielectric lenses. The receiver consists of the horn antenna and SBD detector. Optical modulator is used to allow a narrow-band lock-in detection. Typical modulation frequency was 10 kHz.

In general, when the noise bandwidth increases, the interference effect can be made smaller, but the spatial resolution deteriorates due to the increased lower-frequency/longer-wavelength components. We performed 2D imaging of a clip, etc., hidden in the paper envelope as shown in Fig. 13, to investigate the optimum noise bandwidth by changing the noise bandwidth, ΔB_W, in Fig. 1 (b). At a single frequency with zero noise bandwidth, the image quality is worst due to the interference pattern, while an edge of the image becomes dim with larger noise bandwidth in particular of over 187.5 GHz. So, it can be judged that the noise bandwidth of 62.5 GHz is optimum from the best visibility of the clip.

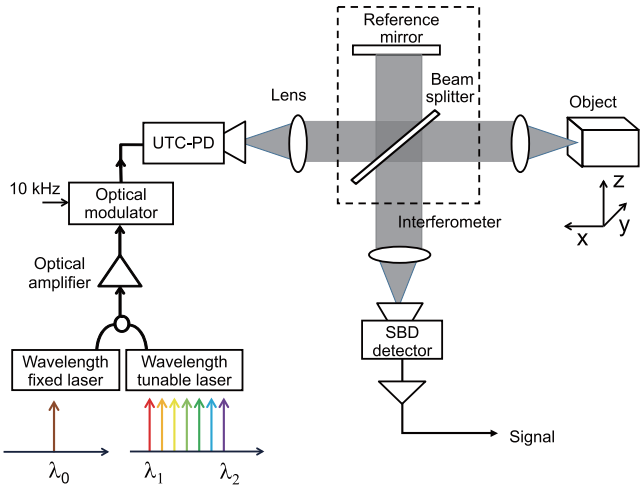

Fig. 14 Block diagram of a THz 3D imaging system based on OCT technique.

3.6 3D Imaging

Figure 14 shows a block diagram of the THz 3D imaging system based on a frequency-domain (swept-source: SS) optical coherence tomography (OCT) technique [31], [32]. It consists of a Mickelson interferometer and a frequency-swept THz source based on Fig. 1 (a). In the SS-OCT system, the spatial (depth) information is obtained by Fourier-transforming the frequency domain interference signals. The theoretical value of depth resolution, Δz, is given as

$$\Delta z = \frac{2\ln 2}{\pi}\frac{\lambda_c^2}{n\Delta\lambda},$$

where λ_c is the center wavelength of the THz source and $\Delta\lambda$ is the spectral width, and n is the refractive index of the object. Our 300-GHz band signal source [31] has a center frequency 325 GHz and FWHM of 87.4 GHz, corresponding to $\lambda_c = 0.92$ mm and $\Delta\lambda = 0.25$ mm, thus, the theoretical depth resolution, Δz, is 1.5 mm in the air ($n = 1$).

THz waves are emitted from the UTC-PD with a horn antenna, and collimated by a dielectric lens. THz waves travel to a beam splitter and are divided in two directions in the ratio of 50/50. One wave goes to the reference mirror and the other is focused onto a test object by the dielectric lens. THz waves, reflected from the reference mirror and backscattered from the test object, travel back to the beam splitter (HRFZ-Si plate with 190-μm thickness), and interference signals are detected by a SBD detector, used as a power detector. Finally, the detected signals are amplified with a preamplifier and a lock-in amplifier. An optical intensity modulator operated at 10 kHz is inserted in front of the photodiode to allow for lock-in detection. A personal computer is used for collecting the transferred data from the lock-in amplifier, and for controlling the components of the system. The 3D imaging is performed by fixing the object on the x-y motorized stage and moving it in steps to the x- and y- directions, performing the so-called raster scan.

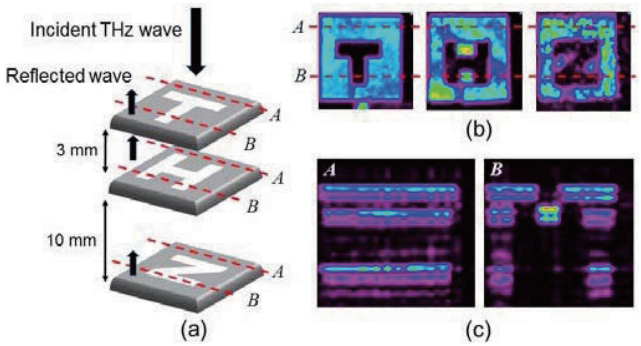

Fig. 15 (a) Object under test: three plastic plates which have hollow holes in the shape of the capital letters T, H, and Z. (b) Measured images of each plate. (c) Tomographic images corresponding to lines *A* and *B*.

Figure 15 shows tomographic images of the object, which consists of three plastic plates which have hollow holes in the shape of the capital letters T, H, and Z. Each plastic plate is 50 mm^2, 1-mm thick, and the distance between the plates is about 3 mm between the first and second and 10 mm between the second and third. Figure 15 (b) shows measured images of each plate. The capital letters T, H and Z are clearly observed. Figure 15 (c) shows tomographic images measured along lines *A* and *B*. As can be seen, each plate consists of two layers corresponding to the front and back sides, respectively, and as a result the position of each plate can be determined.

4. Conclusions

In this paper, we have reviewed recent progress in millimeter-wave and THz measurement systems enabled by photonics, particularly showing how effectively photonics has been used in such applications. Photonics systems using fiber-optics can solve what purely electronic measurement systems are suffering from, such as large loss, dispersion, coupling, and crosstalk as well as bandwidth limitation in the RF signal generation, transmission and detection. Also, in contrast to pulsed/time-domain technologies, CW/frequency-domain approaches make it possible to control frequency and phase more easily and accurately, which can expand application areas.

In order to make these photonics-based millimeter-wave and THz systems more compact, stable and cost-effective, the RF photonics integration technology should be introduced as we have seen in the communications applications [33], [34].

Acknowledgments

The authors would like to express their thanks to H. Nishii and Y. Koda, for their support and help.

Part of this work is supported by the Ministry of Education, Science, Sports and Culture, through the Grant-in-Aid for Scientific Research program (23246067, 23656049, 25709028 and 15K13975).

References

[1] D.H. Auston, "Picosecond optoelectronic switching and gating in silicon," Appl. Phys. Lett., vol.26, no.3, pp.101–103, Feb. 1975.
[2] J. Valdmanis, G.A. Mourou, and C.W. Gabel, "Subpicosecond electro-optic sampling," IEEE J Quantum Electron., vol.19, no.4, pp.664–667, Jan. 1983.
[3] R.B. Marcus ed., Measurement of High-Speed Signals in Solid State Devices (Semiconductors and Semimetals), vol.28, Academic Press, 1990.
[4] T. Nagatsuma, "Measurement of high-speed devices and integrated circuits using electro-optic sampling techniques," IEICE Trans. Electron., vol.E76-C, no.1, pp.55–63, Jan. 1993.
[5] T. Nagatsuma, M. Shinagawa, N. Sahri, A. Sasaki, Y. Royter, and A. Hirata, "1.55-μm photonic systems for microwave and millimeter-wave measurement," IEEE Trans. Microwave Theory and Tech., vol.49, no.10, pp.1831–1839, Oct. 2001.
[6] D. Grischkowsky, S. Keiding, M. van Exter, and Ch. Fattinger, "Far-infrared time-domain spectroscopy with terahertz beams of dielectrics and semiconductors," JOSA B, vol.7, no.10, pp.2006–2015, Oct. 1990.
[7] B.B. Hu and M.C. Nuss, "Imaging with terahertz waves," Optics Letters, vol.20, no.16, pp.1716–1718, Aug. 1995.
[8] M. Tonouchi, "Cutting-edge terahertz technology," Nature Photonics, vol.1, no.2, pp.97–105, 2007.
[9] T. Nagatsuma, "Terahertz technologies: present and future," IEICE Electronics Express, vol.8, no.14, pp.1127–1142, 2011.
[10] T. Nagatsuma, H. Ito, and T. Ishibashi, "High-power RF photodiodes and their applications," Laser Photon. Rev., vol.3, no.1-2, pp.123–137, 2009.
[11] A. Wakatsuki, T. Furuta, Y. Muramoto, T. Yoshimatsu, and H. Ito, "High-power and broadband sub-terahertz wave generation using a J-band photomixer module with rectangular-waveguide output port," Proc. Int. Conf. on Infrared, Millimeter, and Terahertz Waves, pp.1–2, 2008.
[12] M. Jarrahi, "Advanced photoconductive terahertz optoelectronics based on nano-antennas and nano-plasmonic light concentrators," IEEE Transactions on Terahertz Science and Technology, vol.5, no.3, pp.391–397, 2015.
[13] T. Goebel, D. Stanze, B. Globisch, R.J.B. Dietz, H. Roehle, and M. Schell, "Telecom technology based continuous wave terahertz photomixing system with 105 decibel signal-to-noise ratio and 3.5 terahertz bandwidth," Opt. Lett., vol.38, pp.4197–4199, 2013.
[14] J.-Y. Kim, H. Nishi, H.-J. Song, H. Fukuda, M. Yaita, A. Hirata, and K. Ajito, "Compact and stable THz vector spectroscopy using silicon photonics technology," Opt. Express, vol.22, no.6, pp.7178–7185, 2014.
[15] S. Hisatake, G. Kitahara, K. Ajito, Y. Fukada, N. Yoshimoto, and T. Nagatsuma, "Phase-sensitivity terahertz self-heterodyne system based on photodiode and low-temperature-grown GaAs photoconductor at.1.55 μm," IEEE Sensors Journal, vol.13, no.1, pp.31–36, 2013.
[16] S. Hisatake, J.-Y. Kim, K. Ajito, and T. Nagatsuma, "Self-heterodyne spectrometer using uni-traveling-carrier photodiodes for terahertz-wave generators and optoelectronic mixers," Journal of Lightwave Technology, vol.32, no.20, pp.3683–3689, 2014.
[17] S. Hisatake and T. Nagatsuma, "Continuous-wave terahertz field imaging based on photonics-based self-heterodyne electrooptic detection," Opt. Lett., vol.38, no.13, pp.2307–2310, 2013.
[18] S. Hisatake, H.H.N. Pham, and T. Nagatsuma, "Visualization of the spatial–temporal evolution of continuous electromagnetic waves in the terahertz range based on photonics technology," Optica, vol.1, no.6, pp.365–371, 2014.
[19] M. Tsuchiya, A. Kanno, K. Sasagawa, and T. Shiozawa, "Image and/or movie analyses of 100-GHz traveling waves on the basis of real-time observation with a live electrooptic imaging camera,"

IEEE Trans. Microwave Theory Tech., vol.57, no.12, pp.3373–3379, 2009.
[20] H. Togo, A. Sasaki, A. Hirata, and T. Nagatsuma, "Characterization of millimeter-wave antenna using photonic measurement techniques," Int. J. RF Microwave Comput. Aided Eng., vol.14, no.3, pp.290–297, 2004.
[21] M. Hirose, T. Ishizone, and K. Komiyama, "Antenna pattern measurements using photonic sensor for planar near-field measurement at X band," IEICE Trans. Commun., vol.E87-B, no.3, pp.727–734, March 2004.
[22] H.H.N. Pham, S. Hisatake, and T. Nagatsuma, "Far-field antenna characterization in the sub-THz region based on electrooptic near-field measurements," International Topical Meeting on Microwave Photonics/Asia-Pacific Microwave Photonics Conference (MWP/APMP 2014), WC-7, pp.377–380, Oct. 2014.
[23] S. Hisatake and T. Nagatsuma, "Precise terahertz-wave phase measurement based on photonics technology," presented at 39th International Conference on Infrared, Millimeter, and Terahertz waves (IRMMW-THz), AZ, USA, pp.1–2, 14–19 Sept. 2014.
[24] Y. Koda, S. Hisatake, J.-Y. Kim, A. Hirata, K. Ajito, and T. Nagatsuma, "Precise phase measurement of continuous terahertz-wave based on balanced self-heterodyne technique and its application to phase-contrast imaging," Asia-Pacific Microwave Conference (APMC) 2014, pp.1079–1081, Nov. 2014.
[25] R.C. Johnson, H.A. Ecker, and J.S. Hollis, "Determination of far-field antenna patterns from near-field measurements," Proceedings of the IEEE, vol.61, no.12, pp.1668–1694, 1973.
[26] B.B. Hu and M.C. Nuss, "Imaging with terahertz waves," Opt. Lett., vol.20, no.16, pp.1716–1718, 1995.
[27] A.J. Fitzgerald, B.E. Cole, and P.F. Taday, "Nondestructive analysis of tablet coating thickness using terahertz pulsed imaging," J. Pharm. Sci., vol.94, no.1, pp.177–183, 2005.
[28] W.L. Chan, J. Deibel, and D.M. Mittleman, "Imaging with terahertz radiation," Rep. Prog. Phys., vol.70, no.8, pp.1325–1379, 2007.
[29] J. Takayanagi, H. Jinno, S. Ichino, K. Suizu, M. Yamashita, T. Ouchi, S. Kasai, H. Ohtake, H. Uchida, N. Nishizawa, and K. Kawase, "High-resolution time-of-flight terahertz tomography using a femtosecond fiber laser," Optics Express, vol.17, no.9, pp.7533–7539, 2009.
[30] T. Nagatsuma, T. Kumashiro, Y. Fujimoto, K. Taniguchi, K. Ajito, N. Kukutsu, T. Furuta, A. Wakatsuki, and Y. Kado, "Millimeter-wave imaging using photonics-based noise source," Proc. Int. Conf. on Infrared, Millimeter, and Terahertz Waves, pp.1–2, 2009.
[31] T. Ikeo, T. Isogawa, and T. Nagatsuma, "Three dimensional millimeter- and terahertz-wave imaging based on optical coherence tomography," IEICE Transactions on Electronics, vol.E96-C, no.10, pp.1210–1217, 2013.
[32] T. Nagatsuma, H. Nishii, and T. Ikeo, "Terahertz imaging based on optical coherence tomography," OSA Journal Photonics Research, vol.2, no.4, pp.B64–B69, 2014.
[33] A. Suminokura, K. Tsuruda, T. Mukai, M. Fujita, and T. Nagatsuma, "Integration of resonant tunneling diode with terahertz photonic-crystal waveguide and its application to gigabit terahertz-wave Communications," International Topical Meeting on Microwave Photonics/Asia-Pacific Microwave Photonics Conference (MWP/APMP 2014), ThB-3, pp.419–422, Oct. 2014.
[34] G. Carpintero, K. Balakier, Z. Yang, R.C. Guzman, A. Corradi, A. Jimenez, G. Kervella, M.J. Fice, M. Lamponi, M. Chitoui, F. van Dijk, C.C. Renaud, A. Wonfor, E.A.J.M. Bente, R.V. Penty, I.H. White, and A.J. Seeds, "Microwave photonic integrated circuits for millimeter-wave wireless communications," IEEE Journal of Lightwave Tech., vol.32, no.20, pp.3495–3501, 2014.

Tadao Nagatsuma received B.S., M.S., and Ph.D. degrees in electronic engineering from Kyushu University, Fukuoka, Japan, in 1981, 1983, and 1986, respectively. From 1986 to 2007, he was with Nippon Telegraph and Telephone Corporation (NTT), Atsugi, Kanagawa, Japan. Since 2007, he has been a Professor at Graduate School of Engineering Science, Osaka University. His research interests include millimeter-wave and terahertz photonics and their application to sensors and wireless communications. Prof. Nagatsuma is an IEEE Fellow, an IEICE Fellow, and a Fellow of the Electromagnetics Academy, and a Member of the Technical Committee on Microwave Photonics (MTT-3) and Terahertz Technology (MTT-4) of the IEEE Microwave Theory and Techniques Society, and the Microwave Photonics Steering Committee, and serves as an Associate Editor of the IEEE Photonics Technology Letters. He is the recipient of numerous awards including the 1992 IEEE Andrew R. Chi Best Paper Award, the 1997 Okochi Memorial Award, the 1998 Japan Microwave Prize, the 2000 Minister's Award of the Science and Technology Agency, the 2002 and 2011 Asia–Pacific Microwave Conference Prize, the 2004 Yokosuka Research Park Award, the 2006 Asia–Pacific Microwave-Photonics Conference Award, the 2006 European Microwave Conference Prize, the 2007 Achievement Award presented by the IEICE, the 2008 Maejima Award presented by the Post and Telecom Association of Japan, the 2011 Commendation for Science and Technology by the Minister of Education, Culture, Sports, Science and Technology, the 2011 Recognition from Kinki Bureau of Telecommunications, Ministry of Internal Affairs and Communications, the 2012, 2015 Osaka University Presidential Awards for Achievement, the 2013 Nikkei Electronics Japan Wireless Technology Award, and the 2014 IEEE Tatsuo Itoh Award.

Shintaro Hisatake received the M.E. and Ph.D. degrees in electronic engineering from Doshisha University, Kyoto, Japan, in 2000 and 2003, respectively. He was engaged in the development of frequency stabilization and linewidth reduction techniques for visible laser diodes from 2000 to 2003. In 2003, he joined the Graduate School of Engineering Science, Osaka University, Osaka, Japan, where he is currently an Assistant Professor. His research interests include Millimeter-wave and THz wave generation, modulation, and detection based on photonics and their applications to communications, sensing, and imaging. In 2014, he received The Optics Prize for Excellent Papers 2013 from the Japan Society of Applied Physics, and the Osaka University Presidential Awards for Encouragement (2014, 2015). Dr. Hisatake is a member of the IEEE, OSA, IEICE, and JSAP.

Hai Huy Nguyen Pham received the B.E. and M.E. degrees in mechatronics engineering from Ho Chi Minh City University of Technology, Ho Chi Minh City, Viet Nam in 2012 and electronic engineering from Osaka University, Osaka, Japan in 2015, respectively. In 2015, he started Doctoral Course in Graduate School of Engineering Science, Osaka University, Osaka, Japan. His study is involved THz waves measurement using electro-optic sensor. Mr. Nguyen Pham is a student member of IEICE and JSAP.